Tellus
SERIES A DYNAMIC METEOROLOGY AND OCEANOGRAPHY
PUBLISHED BY THE INTERNATIONAL METEOROLOGICAL INSTITUTE IN STOCKHOLM

Tellus (2010), 62A, 173–187

TELLUS

1D+3DVar assimilation of radar reflectivity data: a proof of concept

By OLIVIER CAUMONT*, VÉRONIQUE DUCROCQ, ÉRIC WATTRELOT, GENEVIÈVE JAUBERT and STÉPHANIE PRADIER-VABRE, *CNRM/GAME (Météo-France/CNRS), 31057 Toulouse, France*

(Manuscript received 28 May 2009; in final form 24 November 2009)

ABSTRACT

An original one-dimensional (1-D) retrieval followed by a three-dimensional variational (1D+3DVar) assimilation technique is being developed to assimilate volumes of radar reflectivity data in the high-resolution numerical weather prediction Arome model.

The good performance of the 1-D retrieval is shown for an isolated storm over southwestern France through an observing system simulation experiment. The full method is applied with real data to a flash-flood event, which occurred in a mountainous area. For this complex case, the assimilation of reflectivity data improves short-term precipitation forecasts. The assimilation of reflectivity data has a positive impact on the convective system's dynamics by feeding the cold pool under the storm, which controls the intensity and location of the updrafts. A one-hourly update cycle of 3 h further improves these results.

A sensitivity study is also presented to evaluate the assimilation method for this flash-flood event in different conditions. The smoothing coefficient involved in the 1-D retrieval is shown to have a very small impact on analyses and quantitative precipitation forecasts. The assimilation of reflectivity data is found to be able to cause the creation of a cold pool, which modifies favourably the precipitation quantitative forecast. Finally, results from an 8-d-long assimilation cycle are presented.

1. Introduction

As national weather services are opting for kilometric-scale numerical weather prediction (NWP) systems, new types of observations are needed to initialize these models at similar time and space scales. In this context, radar data are well placed to play a prominent role by providing high-resolution information about precipitation. While radar Doppler velocities seem to be naturally fitted for variational (Sun and Crook, 1997; Lindskog et al., 2004; Montmerle and Faccani, 2009) or Kalman filter-based (Tong and Xue, 2005) assimilation systems, it is still unclear how reflectivity data can be best handled by assimilation systems at cloud-resolving scale. Although four-dimensional variational (4DVar) and Kalman filter-based assimilations show great potential, these methods still suffer from limiting drawbacks. Actually, they require unaffordable computer costs for operational NWP at the kilometric scale, and the underlying assumptions of Gaussian errors and linearity are questionable for the assimilation of reflectivity and related quantities. Also, some impact studies using such reflectivity assimilation methods have shown relatively small benefits in comparison with Doppler velocity data assimilation (e.g. Tong and Xue, 2005; Xue et al., 2006, for a Kalman filter technique and Xiao et al., 2005, 2007; Zhao and Jin, 2008, for a 3DVar method). It is actually questionable whether such direct assimilation of reflectivity data, which are expressed in terms of hydrometeor contents through the observation operator, is the most efficient way of modifying both the thermodynamics and dynamics of the simulated clouds.

In fact, there are assimilation methods of precipitation data that modify other fields than hydrometeor contents. Latent heat nudging, which has been used with success at mesoscale (Jones and Macpherson, 1997), consists in modifying the latent heat release term as a function of the departure between observed and modelled surface precipitation rates. At higher resolution, this method has needed some adjustments because some basic assumptions of the method were violated (Stephan et al., 2008). For instance, at coarser resolutions, all the precipitation is supposed to fall at once in the same column of air, whereas at higher resolutions, atmospheric models usually take into account the advection of hydrometeors by air motions. Other methods use

*Corresponding author.
e-mail: olivier.caumont@meteo.fr
DOI: 10.1111/j.1600-0870.2009.00430.x

reflectivity as input in cloud analysis methods. In this case, it can be used to initialize hydrometeor contents, humidity, and/or latent heat rate (Lin et al., 1993; Ducrocq et al., 2000; Hu et al., 2007). Several studies using such cloud analyses have shown that humidity was one of the most crucial water-related parameters to initialize at cloud scale (Bielli and Roux, 1999; Ducrocq et al., 2002).

At the global scale, one-dimensional variational (1DVar) assimilation in the vertical has been used to retrieve humidity and/or temperature from precipitation observations. This technique has been used alone (Nagarajan et al., 2006) or in combination with some other variational methods. For instance, Marécal and Mahfouf (2002, 2003), and Lopez and Bauer (2007) have first retrieved vertically integrated humidity pseudo-observations through a 1DVar assimilation scheme, which in turn have been assimilated by a 4DVar assimilation system.

Météo-France put into operation Arome (Bouttier, 2003, 2007), its new high-resolution non-hydrostatic model, at the end of 2008. At kilometric scales, and for operational purpose, 4DVar remains unaffordable in computational terms, and the linear hypothesis is not well fulfilled. A 3DVar method has thus been chosen to assimilate observations in Arome. The aim of this article is to present the method that has been devised to assimilate reflectivity in Arome, as well as to demonstrate its potential on a case study. To devise this assimilation method, it would have been tempting to adapt Marécal and Mahfouf's 1DVar+4DVar method to high resolution in the context of the Arome three-dimensional variational (3DVar) assimilation system. However, using 1DVar at the cloud-resolving scale would at least have required the adjoint of Arome mixed-phase microphysical parametrization, which is a difficult and tedious challenge. Rather, to retrieve humidity profiles, it has been decided to follow the Bayesian approach used in the Goddard profiling algorithm (GPROF) to retrieve precipitation rates (Kummerow et al., 1996, 2001; Olson et al., 1996) and latent heating profiles (Olson et al., 1999) from satellite observations and a database of Goddard cumulus ensemble (GCE) simulations. Methods based on the GPROF approach have already been applied successfully to other types of data, for example, for retrieving falling snow profiles from Advanced Microwave Sounder Unit-B (AMSU-B) brightness temperature observations (Kim et al., 2008). So, in a similar manner, the new 1D+3DVar method presented here first converts reflectivity into humidity, based on the GPROF approach. Then, humidity is assimilated as pseudo-observations with Arome 3DVar assimilation system, which is also used to assimilate other observations.

This paper is organized as follows. First, the 1D+3DVar method is presented in detail in Section 2. Then, the performance of the 1-D retrieval, which is the first step of the 1D+3DVar method, is assessed through an observing system simulation experiment (OSSE) in Section 3. Section 4 unfolds results of 1D+3DVar assimilations of real data for a case of extreme precipitation over southern France. In Section 5, the sensitivity of the method to different configurations is investigated for the same case. Results of an eight-day-long assimilation cycle are shown in Section 6. Conclusions follow in Section 7.

2. Description of the 1D+3DVar assimilation method

The sequence of operations performed in the 1D+3DVar assimilation method is illustrated in Fig. 1. The first step is a retrieval of vertical profiles of pseudo-observations of humidity from reflectivity vertical profiles. The second step consists of assimilating the pseudo-observations built during the first step with a conventional 3DVar data assimilation system.

2.1. 1-D retrieval

The 1-D retrieval uses a Bayesian method based on GPROF (Kummerow et al., 2001). GPROF makes use of a large database of simulated vertical profiles of consistent synthetic observations and parameters to find the most probable value of the parameter to retrieve according to the observed vertical profile. In the following, this algorithm is briefly recalled, then the 1-D retrieval used in this study is presented.

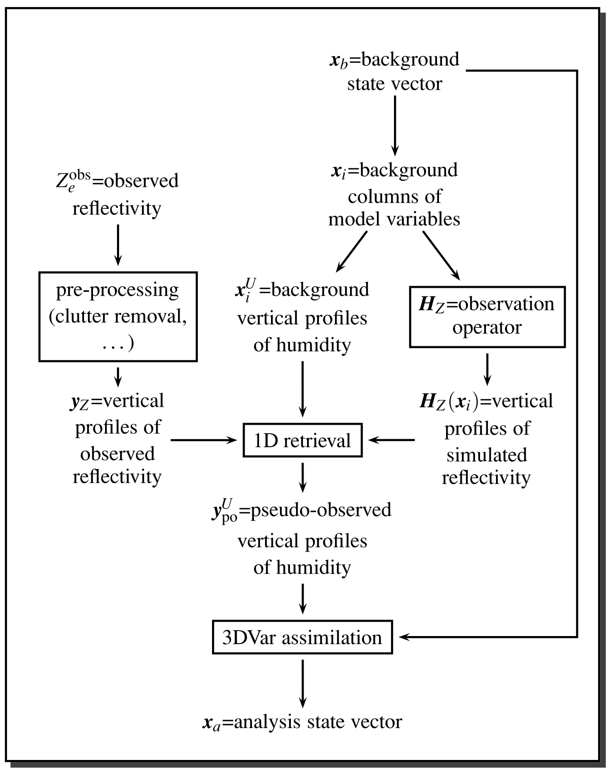

Fig. 1. Flow chart that shows the sequence of operations performed in the 1D+3DVar assimilation of reflectivity data.

Let the vector $\boldsymbol{x}$ represent the model state vector of a vertical profile to retrieve, $\boldsymbol{x}_{\text{true}}$ denote the true state vector, and the vector $\boldsymbol{y}_0$ represent a set of available observations. The best estimate of $\boldsymbol{x}$ given the set of observations $\boldsymbol{y}_0$ is (see, e.g. Lorenc, 1986)

$$\boldsymbol{E}(\boldsymbol{x}) = \int \boldsymbol{x}\mathrm{P}(\boldsymbol{x} = \boldsymbol{x}_{\text{true}}|\boldsymbol{y} = \boldsymbol{y}_0)\,\mathrm{d}\boldsymbol{x}\,. \tag{1}$$

Using Bayes' theorem, it can be rewritten as

$$\boldsymbol{E}(\boldsymbol{x}) = \int \boldsymbol{x}\mathrm{P}(\boldsymbol{y} = \boldsymbol{y}_0|\boldsymbol{x} = \boldsymbol{x}_{\text{true}})\mathrm{P}(\boldsymbol{x} = \boldsymbol{x}_{\text{true}})\,\mathrm{d}\boldsymbol{x}\,. \tag{2}$$

Then, let us assume that the errors in the observations and the simulated observations are Gaussian and uncorrelated. In this case,

$$\begin{aligned}&\mathrm{P}(\boldsymbol{y} = \boldsymbol{y}_0|\boldsymbol{x} = \boldsymbol{x}_{\text{true}})\\ &\quad\propto \exp\left\{-\frac{1}{2}\left[\boldsymbol{y}_0 - \boldsymbol{h}(\boldsymbol{x})\right]^{\mathrm{T}}(\mathbf{O}+\mathbf{S})^{-1}[\boldsymbol{y}_0 - \boldsymbol{h}(\boldsymbol{x})]\right\}\,,\end{aligned} \tag{3}$$

where $\mathbf{O}$ and $\mathbf{S}$ are the observation and simulation error covariance matrices, respectively, and $\boldsymbol{h}$ is the observation operator that simulates observations from the model. At this stage, the original approach taken in GPROF is to assume that simulated profiles from a large database 'occur with nearly the same relative frequency as those found in nature, or at least with the same frequency as those found in the region where the retrieval method is to be applied' (Olson et al., 1996). Using this assumption, eq. (2) can be approximated by

$$\boldsymbol{E}(\boldsymbol{x}) = \sum_i \boldsymbol{x}_i \frac{W_i}{\sum_j W_j} \tag{4}$$

with

$$W_i \equiv \exp\left\{-\frac{1}{2}\left[\boldsymbol{y}_0 - \boldsymbol{h}(\boldsymbol{x}_i)\right]^{\mathrm{T}}\mathbf{R}^{-1}\left[\boldsymbol{y}_0 - \boldsymbol{h}(\boldsymbol{x}_i)\right]\right\}\,, \tag{5}$$

where $\boldsymbol{x}_i$ is a profile taken from the database.

In this study, the main difference is that the database consists of model forecasts, valid for the observation time, and located in the neighbourhood of each observed vertical profiles. Indeed, it is expected that, in most cases, the model will be able to produce something similar to what is observed, but at a wrong location. By looking in the neighbourhood of the observation point, rather than in a large database gathering various meteorological situations, the method uses pseudo-observations, which are consistent with the meteorological situation of the day.

The observed reflectivities are available in the plan position indicator (PPI) planes and are interpolated to a Cartesian grid in the horizontal directions. In doing so, observations can be treated as vertical profiles. In this study, vertical profiles of relative humidity are retrieved instead of the whole model state vector for GPROF. The method might be used with other types of pseudo-observations, however. Thus, for each observed vertical profile of reflectivity ($\boldsymbol{y}_Z$), a vertical profile of pseudo-observations of relative humidity ($\boldsymbol{y}_{\text{po}}^U$) is given by an expression similar to eq. (4)

$$\boldsymbol{y}_{\text{po}}^U = \sum_i \boldsymbol{x}_i^U \frac{W_i}{\sum_j W_j}\,, \tag{6}$$

with

$$W_i \equiv \exp\left\{-\frac{1}{2}[\boldsymbol{y}_Z - \boldsymbol{H}_Z(\boldsymbol{x}_i)]^{\mathrm{T}}\mathbf{R}_Z^{-1}[\boldsymbol{y}_Z - \boldsymbol{H}_Z(\boldsymbol{x}_i)]\right\}\,, \tag{7}$$

where $\boldsymbol{x}_i$ are model columns taken from the model background state in the vicinity of the observed column, $\boldsymbol{x}_i^U$ are the corresponding vertical profiles of model relative humidity interpolated at each observation elevation, $\boldsymbol{H}_Z(\boldsymbol{x}_i)$ are the corresponding vertical profiles of simulated reflectivities, and $\mathbf{R}_Z$ is the covariance matrix of observation and observation operator errors.

The radar simulator described by Caumont et al. (2006) is used as the observation operator for reflectivity $\boldsymbol{H}_Z$. It takes into account the effects of beam bending and curvature of the Earth by using the 4/3 Earth radius model introduced by Schelleng et al. (1933). Vertical beam broadening is taken into account by computing several ray paths and weighting the corresponding simulated observations by the antenna's directivity function. The simulated reflectivity, in dBZ, is computed on each ray path from the mixing ratios of rainwater, snow, graupel and pristine ice, in accordance with the atmospheric model microphysical parametrization. Each profile of simulated reflectivity is computed as if it were exactly at the observation location, so that it can be properly compared with the observation.

For the sake of simplicity, the $\mathbf{R}_Z$ matrix is chosen diagonal with a diagonal term equal to $n\sigma_Z^2$, where n is the number of observations in a vertical profile, and σ_Z is the standard deviation of observation and observation operator errors. In our experiments, σ_Z is set to 0.2 dB, unless stated otherwise. The sensitivity of the method to this parameter is discussed in Section 5.1.

According to eq. (6), each vertical profile of pseudo-observations is therefore a linear combination of neighbouring vertical profiles taken from the model background state. The weight associated with each neighbouring vertical profile is a function of the difference between observed and simulated reflectivities. The smaller this difference, the larger the weight is. The neighbours are all model columns $\boldsymbol{x}_i$ within a square window centred on the observation $\boldsymbol{y}_Z$. A moving window of 21×21 columns (i.e. $52.5 \times 52.5\,\mathrm{km}^2$) centred on each observed vertical profile of reflectivities is used as a database in the Bayesian method to compute pseudo-observations of relative humidity.

The main drawback of this method is that resulting vertical profiles will be limited to what the model is able to produce at the time of analysis. For instance, if developed convective cells are observed, while no convection is triggered in the model, the method will not be able to find neighbouring columns with significant reflectivities. Where reflectivity is observed (i.e. $Z > 0\,\mathrm{dBZ}$), but null reflectivity is simulated by the model because hydrometeor contents are negligible, a 'humidity adjustment' (HA) raises the value of relative humidity to 100% to prevent this effect. This adjustment is not applied below the model condensation level to allow the precipitation to evaporate in unsaturated air below the cloud base. Thus, in the corresponding pseudo-observations, humidity is set to 100% below the model condensation level, while it has no value below. Saturating gridpoints in cloudy areas is reasonable at the kilometric scale; such adjustment methods have been used with success in the past by Lin et al. (1993) and Ducrocq et al. (2000).

2.2. *3DVar assimilation*

Each retrieved vertical profile of pseudo-observations is then assimilated, as any other observations, with the Arome 3DVar data assimilation system, which is the same as the Aladin assimilation system (Fischer et al., 2005). At the time of this study, the Arome system was not yet available. For the experiments presented here, the choice was made to use the Aladin 3DVar as data assimilation system, and to emulate the forecasting step by using the mesoscale non-hydrostatic (Meso-NH) model (Lafore et al., 1998) in order to produce the background for the next analysis. The use of Meso-NH was motivated by the fact that this model has an advanced representation of the water cycle, with five hydrometeor types (cloudwater, rainwater, primary ice, snow and graupel) governed by a bulk microphysics parametrization, which is implemented in the Arome model. Moreover, in this study it is run at 2.5-km horizontal resolution, which is the same as that of the operational version of Arome, and convection is explicitly resolved as in Arome.

In 3DVar, the following cost function is minimized for a state vector $\boldsymbol{X}$ that represents all model variables at all gridpoints

$$J(\boldsymbol{X}) = \frac{1}{2}(\boldsymbol{X} - \boldsymbol{X}_b)^{\mathrm{T}}\mathbf{B}^{-1}(\boldsymbol{X} - \boldsymbol{X}_b) + \frac{1}{2}[\boldsymbol{Y} - \boldsymbol{H}(\boldsymbol{X})]^{\mathrm{T}}\mathbf{R}^{-1}[\boldsymbol{Y} - \boldsymbol{H}(\boldsymbol{X})], \tag{8}$$

where $\boldsymbol{X}_b$ is the background state vector, $\boldsymbol{Y}$ is a set of observations, $\boldsymbol{H}$ is the observation operator, $\mathbf{B}$ is the background error covariance matrix, and $\mathbf{R}$ is the observation error covariance matrix. The $\mathbf{B}$ matrix has been specially designed for high horizontal resolution. It is based on an extrapolation of the $\mathbf{B}$ matrix used by Aladin at 9.6-km horizontal resolution, but with increased covariances in the lower levels to reduce the effect of the geostrophic balance (Jaubert et al., 2005). In this study, horizontal correlation lengths are further reduced by a factor of 5, while horizontal standard deviations are five times larger to counterbalance this effect. Figure 2 shows the statistics for unbalanced humidity for the operational Aladin model at 9.6-km horizontal resolution, and for the hybrid system at 2.5-km horizontal resolution, respectively. Unbalanced humidity is the part of humidity that is not correlated with other control variables through a physical constraint like the geostrophic balance (see Fischer et al., 2005). In particular, the sharper correlation curve at 0-km range for the hybrid system denotes smaller correlation lengths than for the Aladin model at 9.6-km horizontal resolution (e.g. Berre, 2000). The $\mathbf{B}$ matrix that is used in the current operational version of Arome is based on an ensemble of Arome forecasts, which was not yet available at the time of this study. For this operational $\mathbf{B}$ matrix, covariances in the lower levels are also increased and correlation lengths are reduced in comparison with the Aladin $\mathbf{B}$ matrix, but not as much as for the

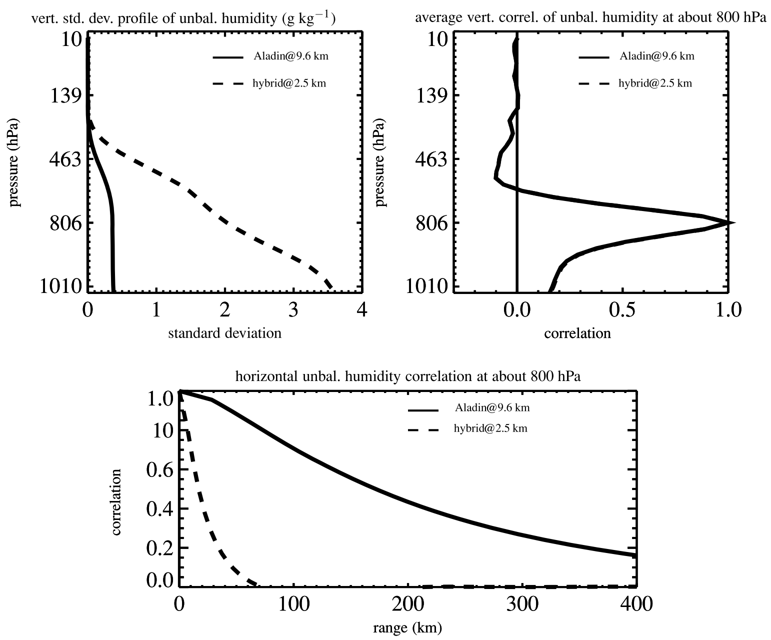

Fig. 2. Background error statistics for unbalanced humidity.

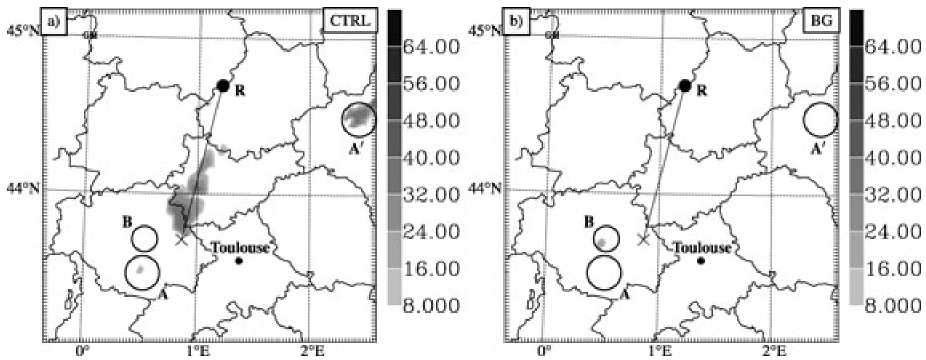

Fig. 3. Horizontal cross-sections of reflectivity at 4.5 km MSL (dBZ) at 1615 UTC on 9 October 2004: (a) CTRL; (b) BG. The location of the fictious radar R (44.7°N, 1.2°E, 230 m MSL) is marked by a big black dot. See text for the meaning of the other letters and symbols.

B matrix used here. Since both systems have the same vertical resolutions, it is reasonable to assume that the average vertical resolutions are also the same (upper right-hand panel, in Fig. 2).

The observation error covariance matrix is diagonal and the associated error for relative humidity is set to 12%. In some experiments, surface data are included along with the humidity pseudo-observations; they include mesonet temperature, pressure, relative humidity and 10-m wind observations.

3. Assessment of the 1-D retrieval through an OSSE

3.1. Experimental setup

The ability of the 1-D retrieval has been assessed through the use of an OSSE, which is a well-known technique to evaluate the benefit of including a new observation type in an assimilation system (see, e.g. Arnold and Dey, 1986). Here, two different simulations are used. The 'observed' reflectivies are simulated from a first simulation (hereafter referred to as 'CTRL'), which is considered as the true state of the atmosphere. The background is provided by a second simulation (hereafter referred to as 'BG'). The retrieved field of pseudo-observed relative humidity can then be compared with that of CTRL. This methodology has the advantage of disregarding both model and observation errors that might affect results.

The chosen case is a storm that occurred on 9 October 2004 over southwestern France. The meteorological situation is characterized by isolated convective cells that develop in a southwesterly flow. This case is particularly interesting to check whether the 1-D retrieval is able to displace the signature in humidity associated with convective cells when they are wrongly located in the background. The two simulations are carried out with the Meso-NH model. The BG simulation starts from an Arpege (Météo-France global model) analysis at 1200 UTC. The CTRL simulation starts from a mesoscale analysis of mesonet surface observations (Ducrocq et al., 2000) applied to the Arpege analysis at 1200 UTC. The 1-D retrieval is performed at 1615 UTC on 9 October 2004. At this time, deep convective cells, organized along a line, are present in CTRL, whereas shallow cells are present in BG (Fig. 3). Moreover, cells are not located at the same locations in the two simulations.

Reflectivities from a fictious *S*-band radar located to the north of Toulouse (R in Fig. 3) with 13 elevations between 0.4° and 18°, and a maximum range of 260 km, are simulated from CTRL. The synthetic observations are arranged on 256 × 256 Cartesian frames centred on the radar with 2-km horizontal resolution.

3.2. Results

The retrieved humidity is shown in Fig. 4c and compared to the BG and CTRL ones in Figs. 4a and b. For the sake of a better representation, pseudo-observations in Fig. 4c have been blended in the relative humidity field of BG through a simple bilinear interpolation. It can be seen that the 1-D retrieval is able to force saturation where convective cells are present in CTRL but not in BG (A and A′ areas in Figs. 3a, b and 4a–c). Conversely, where convective cells are present in BG but not in CTRL, the 1-D retrieval is able to generate pseudo-observations, which are drier than in BG (B area in Figs. 3a, b and 4a–c). Since the cells in BG are surrounded by relatively dry areas without hydrometeors, the Bayesian method is able to combine them and produce an average vertical profile that reflects the model state outside of the convective cell. In Fig. 4d, the difference between pseudo-observations and BG is plotted. It is clear from this figure that the 1-D retrieval has been able to displace the signature in humidity of the convective cells eastwards, in accordance with the observations.

4. 1D+3DVar assimilation of real observations

The full data assimilation procedure was applied to a severe flash-flood event that occurred on 8–9 September 2002 in southeastern France. This case is hereafter referred to as 'the Gard case'. This case has been much documented from both meteorological and hydrological points of views (Chancibault et al.,

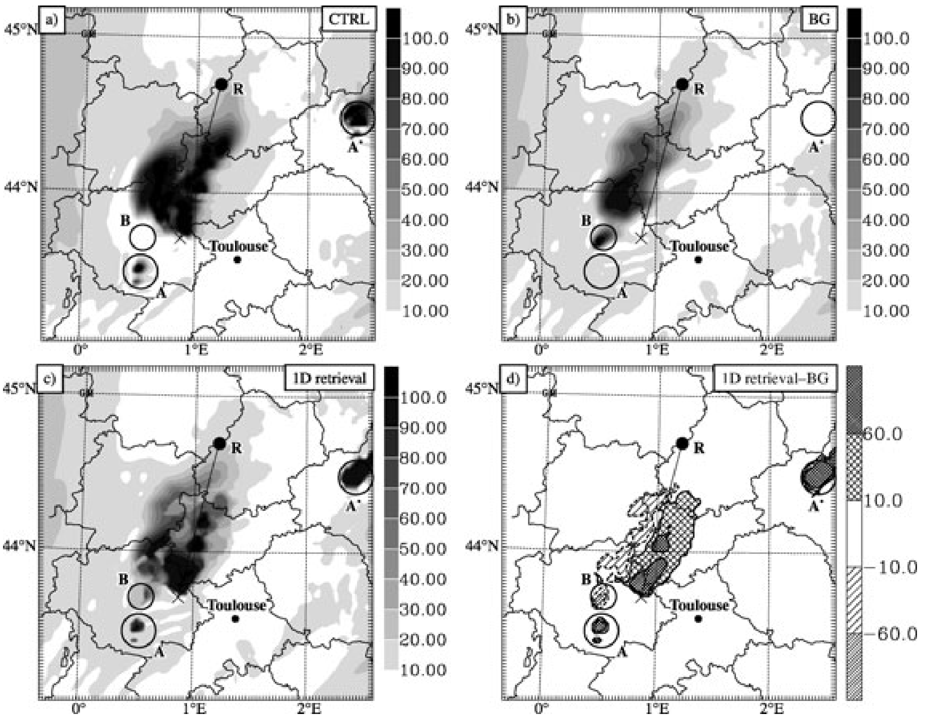

Fig. 4. Horizontal cross-sections of relative humidity (%) at 4.5 km MSL at 1615 UTC on 9 October 2004: (a) CTRL; (b) BG; (c) 1-D retrieval; (d) difference between the 1-D retrieval and BG.

2006; Nuissier et al., 2008; Ducrocq et al., 2008, among others), and a more detailed description of this event is in particular provided by Delrieu et al. (2005). This event is characterized by a mesoscale convective system (MCS) that stayed almost over the same area from 1200 UTC, 8 September, to 1200 UTC, 9 September.

Ducrocq et al. (2008) have shown that the mesoscale conditions associated with the MCS when it was over the Gard plains (i.e. from 1200 UTC to 2100 UTC, 8 September) were (i) a southerly warm, moist low-level jet and (ii) a low-level cold pool under the convective part resulting from the evaporation of precipitation near the ground. They have shown that the cold pool played a prominent role by forcing the low-level jet to rise at its leading edge, and thereby explained the location of precipitation maxima over the Gard plains. We focus here on this phase.

4.1. Experimental setup

As a reference, a simulation is started from a 3DVar analysis of mesonet surface data (2-m temperature and relative humidity, and 10-m wind) at 2.5-km horizontal resolution applied to the Arpege analysis at 1200 UTC, when convection is already organized over the area of interest (surface data are not assimilated by the Arpege assimilation system). Taking into account the surface observations is necessary because it was shown by Nuissier et al. (2008) and Ducrocq et al. (2008) that the low-level cold pool had to be represented in the initial conditions at 1200 UTC to allow for an acceptable simulation of this event. This simulation is hereafter referred to as 'REF12'.

The reflectivity observations considered here are measured by the Bollène S-band radar. This radar scans the atmosphere at 13 elevations between 0.4° and 18° every 15 min. Its maximum range is 260 km. The data are available on 256×256 Cartesian grids at the resolution of 2 km. A quality index is associated with each gridpoint so as to remove non-meteorological data. For instance, ground clutter is detected by comparing observations with a climatological map of ground echoes and comparing the standard deviation of reflectivities with a threshold (Parent du Châtelet et al., 2001). The Surfillum software (Delrieu et al., 1995) is used to identify beam blockage.

A simulation, hereafter referred to as 'RAD12', starts from an analysis at 1200 UTC that takes into account observed reflectivities in addition to surface data. This is done by applying the 1-D retrieval to the 1200 UTC Arpege analysis. Then, the resulting pseudo-observations of relative humidity are assimilated along with the mesonet surface data by the assimilation system at a horizontal resolution of 2.5 km.

In addition, an assimilation cycle is performed for which only reflectivity data are assimilated every hour between 1300 UTC and 1500 UTC. Background fields for analyses between 1300 UTC and 1500 UTC are provided by the 1-h Meso-NH forecasts. The simulation that starts from the last analysis at 1500 UTC is hereafter called 'RAD15' (see Fig. 5).

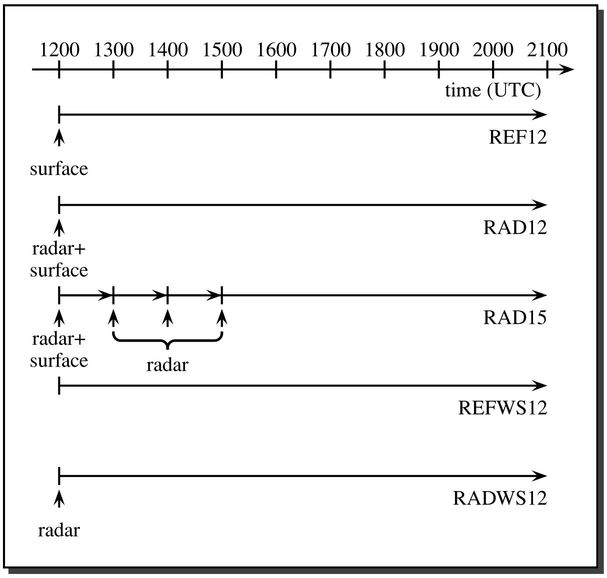

Fig. 5. Characteristics of experiments.

4.2. *Results*

Figure 6 shows the 6-h accumulated surface rainfall between 1500 UTC and 2100 UTC on 8 September 2002 observed by the rain gauge network, the Nîmes radar, and simulated by REF12, RAD12 and RAD15. The radar estimate (Fig. 6b) helps identifying the structure of convective precipitation occurring over the Gard plains. It should be noted that precipitation associated with the front, to the northwest of the domain, are out of the Nîmes radar range, and therefore do not appear in this figure. Scores against rain gauge observations, including bias, root mean square error (RMSE), and correlation coefficient (*R*), have also been computed for each simulation, as well as categorical skill scores such as equitable threat score (ETS) and frequency bias (FBIAS) (Fig. 7). To compute these scores, data have been averaged over boxes of 0.3° of longitude by 0.2° of latitude.

By comparing Figs. 6a–d, one can readily see that RAD12 produces more accurate rainfall totals than REF12. Precipitations are more intense in RAD12, especially over the Gard plains, where rainfall totals are maximal. The bias score, which reduces from 3.3 mm in REF12, to 1.3 mm in RAD12, confirms this result. By moistening the middle and upper troposphere, the assimilation of reflectivity data favours the formation of precipitation. In RAD12, the area of high precipitation that reaches the ground is larger than in REF12, as illustrated by Fig. 8a. In experiment RAD12, the increase in precipitation also causes more evaporation in subsaturated low layers than in REF12. The cooling associated with the evaporation of rainfall leads to the enhancement of the cold pool under the convective system. The time evolution of this cold pool is shown in Fig. 8b. For that, the surface with 2-m AGL virtual potential temperature smaller than 295 K has been estimated. Figure 9 which displays low-level virtual potential temperature, shows that the 295-K threshold allows to delineate the cold pool without ambiguity. Figures 8b and 9a–c show that the cold pool is more intense and extends over a larger area in RAD12 than in REF12, in better agreement with surface measurements. In particular, it is apparent in Figs. 9a–c that REF12 is not able to maintain a cold pool as extensive in the southwest-northeast direction as in the observations. Upward forcing is thus more intense at the leading edge of the cold pool in RAD12 (Figs. 9b and c), resulting in a positive feedback on the intensification of precipitation. Continuous skill scores (Fig. 6) confirm that the assimilation of reflectivity data has a positive impact on the quantitative precipitation forecast (QPF) in terms of both position and intensity. RAD12 outperforms REF12 in terms of ETS for all thresholds (Fig. 7a). FBIAS shows that accumulated precipitation is underforecast for all thresholds for REF12 and RAD12 (Fig. 7b). Although FBIAS is similar for REF12 and RAD12, RAD12 shows slightly more skill for thresholds above 4 mm.

In RAD15, the features identified in RAD12 are more pronounced. The extent of the cold pool and the upward forcing at its leading edge are larger than in RAD12 (Figs. 8a and b). In fact, the cold pool corresponds even better to observations since it spreads throughout the Rhone valley and also to the southeast in the Hérault region (see Fig. 6a to locate the Rhone valley and the Hérault region). In RAD15, the precipitation are more intense than in RAD12. As a result, BIAS becomes negative, denoting an overestimation of precipitation in comparison with rain gauge observations, but the RMSE is unchanged and correlation is improved, compared with RAD12. In terms of ETS, RAD15 is overall better than REF12. RAD12 is better than RAD15 for lower thresholds and conversely, though (Fig. 7a). FBIAS is very close to 1 for RAD15, except that RAD15 tends to overforecast highest precipitation amounts (Fig. 7b).

5. Sensitivity tests

In this section, we investigate the dependence of the 1D+3DVar assimilation method on the prescribed value of σ_Z (see Section 2.1). Also, we evaluate whether a cold pool can still be created during the forecast when reflectivity is assimilated without surface data.

5.1. *Sensitivity of the 1D+3DVar assimilation method to σ_Z*

First, the sensitivity of the 1D+3DVar assimilation method to σ_Z is investigated to examine whether the performance of the 1D+3DVar assimilation method depends dramatically upon the prescribed value of the observation and observation operator error standard deviation. σ_Z can also be interpreted as a smoothness coefficient, as illustrated by the following example. If only two background model columns are considered, the corresponding pseudo-observation can be obtained through the following

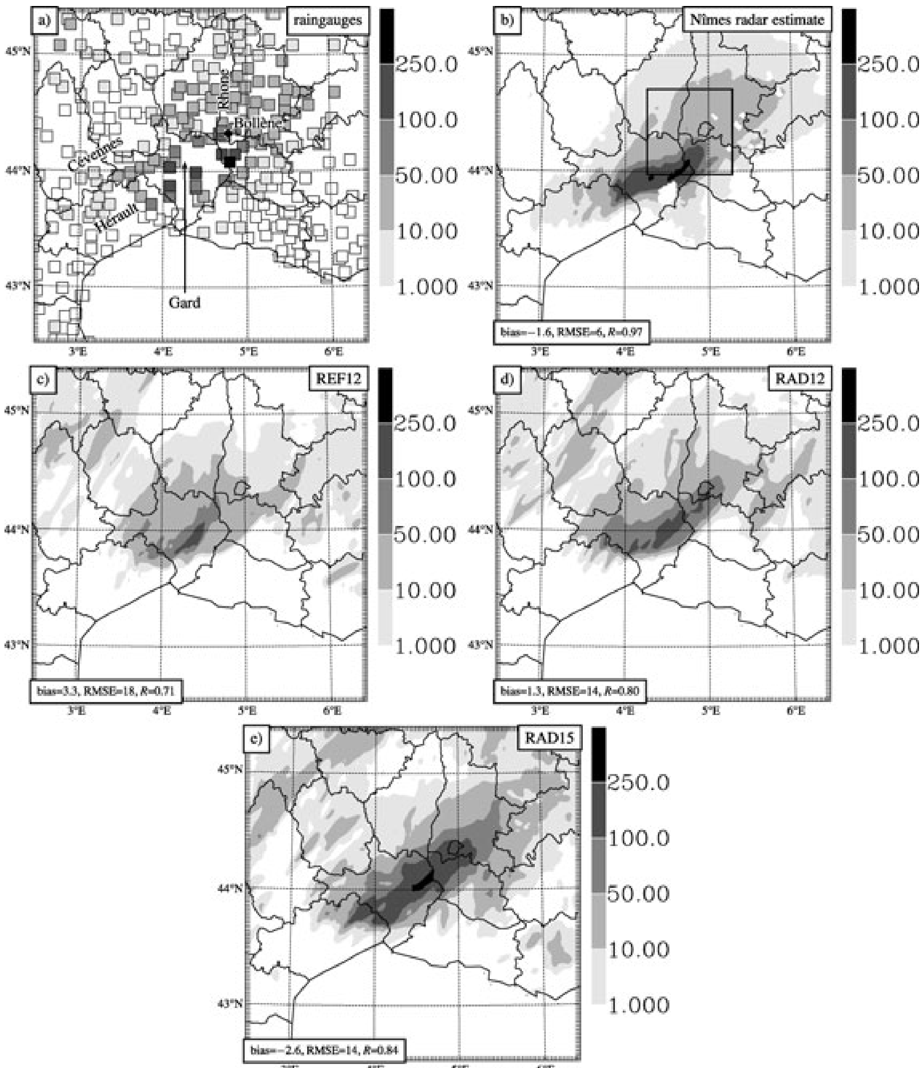

Fig. 6. Six-hour accumulated rainfall (mm) between 1500 UTC and 2100 UTC on 8 September 2002. (a) rain gauge observations, (b) Nîmes radar estimate, and (c–e) simulated. Bias (mm), root mean square error (RMSE, mm), and correlation coefficient (R) against rain gauge observations. See text for the names of the simulations and parameters. The square in (b) refers to the domain plotted in Fig. 10.

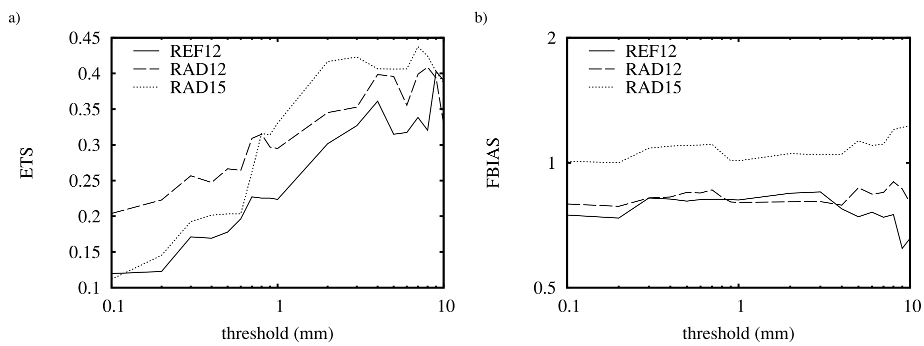

Fig. 7. (a) Equitable threat score and (b) frequency bias for 6-h accumulated precipitation between 1500 UTC and 2100 UTC on 8 September 2002. Perfect scores are 1 in both cases.

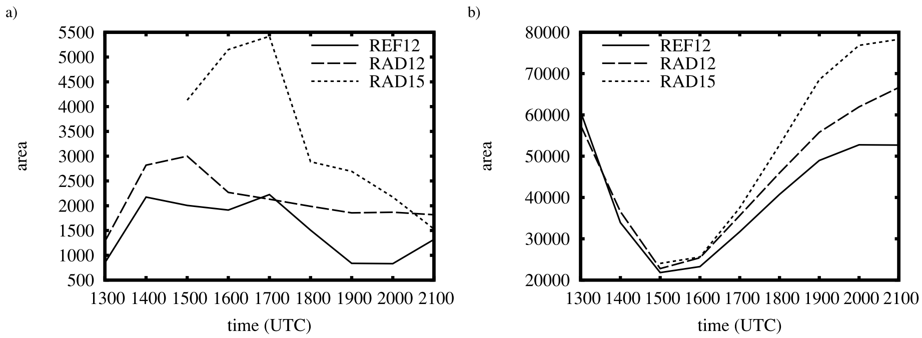

Fig. 8. Time series of: (a) area (km^2) for which surface rainfall rate exceeds 20 mm h^{-1}; (b) area for which θ_v is below 295 K at 2 m AGL.

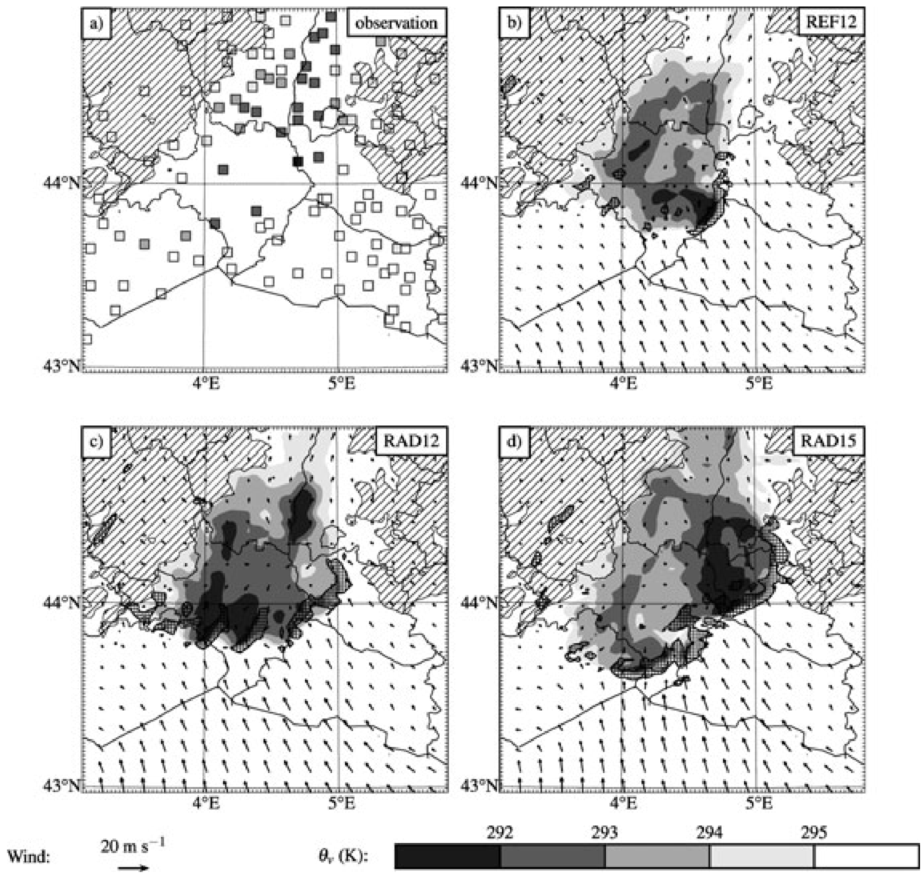

Fig. 9. (a) Virtual potential temperature (θ_v, in K) at 2 m AGL observed by the mesonet network at 1900 UTC on 8 September 2002. (b–d) Simulated virtual potential temperature (θ_v, in K) at 2 m AGL, vertical velocity greater than 1 m s^{-1} at 2 km MSL (square hatch), and 10-m wind at 1900 UTC on 8 September 2002. Diagonal hatches represent the orography above 750 m AGL.

formula:

$$\boldsymbol{y}_{\mathbf{po}} = \frac{\boldsymbol{x}_1 \exp\left(-\dfrac{d_1^2}{2n_{\text{obs}}\sigma_Z^2}\right) + \boldsymbol{x}_2 \exp\left(-\dfrac{d_2^2}{2n_{\text{obs}}\sigma_Z^2}\right)}{\exp\left(-\dfrac{d_1^2}{2n_{\text{obs}}\sigma_Z^2}\right) + \exp\left(-\dfrac{d_2^2}{2n_{\text{obs}}\sigma_Z^2}\right)}, \tag{9}$$

with

$$d_i^2 \equiv \left[\boldsymbol{y}_Z - \boldsymbol{H}_Z(\boldsymbol{x}_i)\right]^{\mathrm{T}} \left[\boldsymbol{y}_Z - \boldsymbol{H}_Z(\boldsymbol{x}_i)\right], \qquad i \in \{1;2\}. \tag{10}$$

Now, suppose that $d_1 < d_2$ (the observed reflectivity profile resembles more column 1 than column 2). Let ϱ denote the ratio between the weight of the model column that resembles most the observation and the weight of the model column that differs more from the observation. Then

$$\varrho = \exp\left(\frac{d_2^2 - d_1^2}{2n_{\text{obs}}\sigma_Z^2}\right). \tag{11}$$

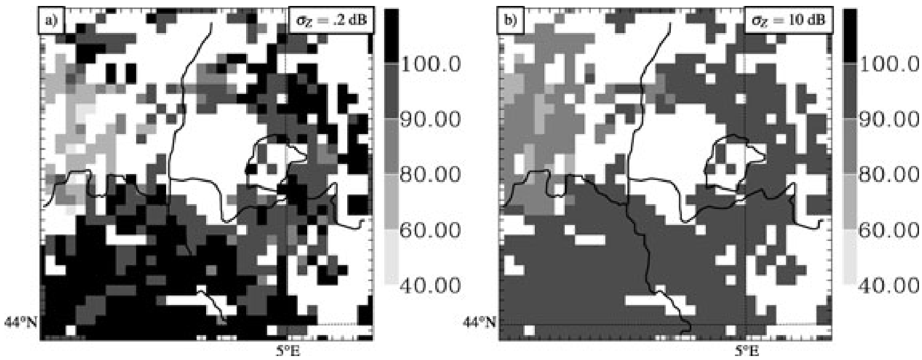

Fig. 10. Constant Altitude PPI (CAPPI) of relative humidity pseudo-observations (%) at 700 ± 50 hPa for RAD15 with a) $\sigma_Z = .2$ dB, b) $\sigma_Z = 10$ dB (the domain location is indicated by a square in Fig. 6b).

It means that the smaller σ_Z, the larger ϱ, that is, the relative weight of the column that is closer to the observation is more important, and vice versa. A direct generalisation leads to the conclusion that too large σ_Z will bring quite similar weights to all columns, whereas too small σ_Z will favour the columns that resemble most the observation.

Experiments have been carried out with various values for σ_Z ranging from 0.2 up to 10 dB. Figure 10 shows relative humidity pseudo-observations at 700 ± 50 hPa for RAD15 with $\sigma_Z = 0.2$ dB and $\sigma_Z = 10$ dB. As expected, it can be noted that the field of pseudo-observations is smoother when $\sigma_Z = 10$ dB. Also, when $\sigma_Z = 10$ dB, only few pseudo-observations come from the humidity adjustment in comparison with $\sigma_Z = 0.2$ dB. Instead, they are computed through the Bayesian retrieval. That is because the weights associated with each model background column in the Bayesian retrieval increase with σ_Z. When all the weights are too small, it means that no column in the background is close enough to the observations, and therefore no pseudo-observation is produced. When there is precipitation, the humidity adjustment produces a saturated profile in that case, though. So, when σ_Z increases, new pseudo-observations are produced in non-precipitating areas, and some saturated pseudo-observations produced by the humidity adjustment are produced by the Bayesian method instead. As a result, the total number of pseudo-observations produced by the 1-D retrieval increases slowly with σ_Z up to about 1 dB. Figure 11 shows the distribution of pseudo-observations produced by the Bayesian method and the humidity adjustment. In this figure, pseudo-observations are separated into 'active' pseudo-observations, that is, that are really assimilated, and 'rejected' pseudo-observations, that is, that are rejected because they fail the quality-control checks. When σ_Z increases, the number of pseudo-observations computed by the Bayesian method increases, while the number of pseudo-observations computed by the humidity adjustment decreases down to 0. For $\sigma_Z \geq 1$ dB, only the Bayesian method produces pseudo-observations. Above this threshold, the number of rejected and active pseudo-observations remains approximately the same.

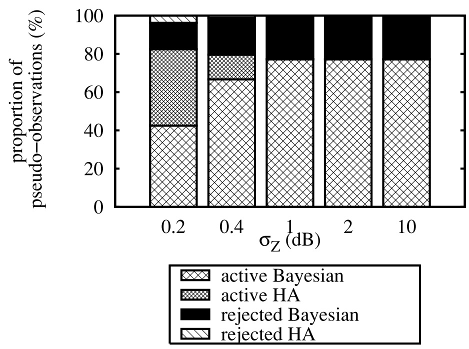

Fig. 11. Distribution of pseudo-observations entering the 3DVar assimilation system for RAD15 for various values of σ_Z. 'Bayesian' refers to pseudo-observations produced by the Bayesian method, while 'HA' refers to pseudo-observations produced by the humidity adjustment.

In spite of notable changes in the distribution and number of pseudo-observations, the value of σ_Z has a negligible impact on integrated water vapour analysis increments (see Fig. 12, for RAD15 with two different values of σ_Z). As a result, quantitative 6-h precipitation forecasts do not differ much in pattern, intensity, and scores, as seen in Fig. 13 for experiment RAD15 with various values of σ_Z (to compare with Fig. 6e with the default value $\sigma_Z = 0.2$ dB). ETS and FBIAS are also similar for all experiments (not shown).

So, for this case, different values of σ_Z impact pseudo-observations, but have a very small impact on analyses and QPF, even after a one-hourly update assimilation cycle of 3 h. A plausible explanation is that during the 3DVar assimilation step, the *B* matrix structure functions smooth increments with a similar effect whatever the value of σ_Z.

5.2. *Role of the assimilation of surface data*

In the previous experiments, surface data have been assimilated at 1200 UTC. The reason for doing so was to describe correctly the cold pool under the storm that is present in the observations,

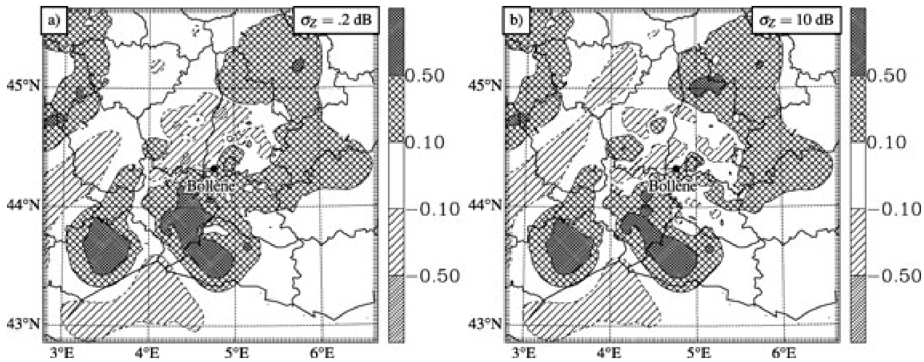

Fig. 12. Vertically integrated water vapour analysis increments (cm) for RAD15 with two different values of σ_Z.

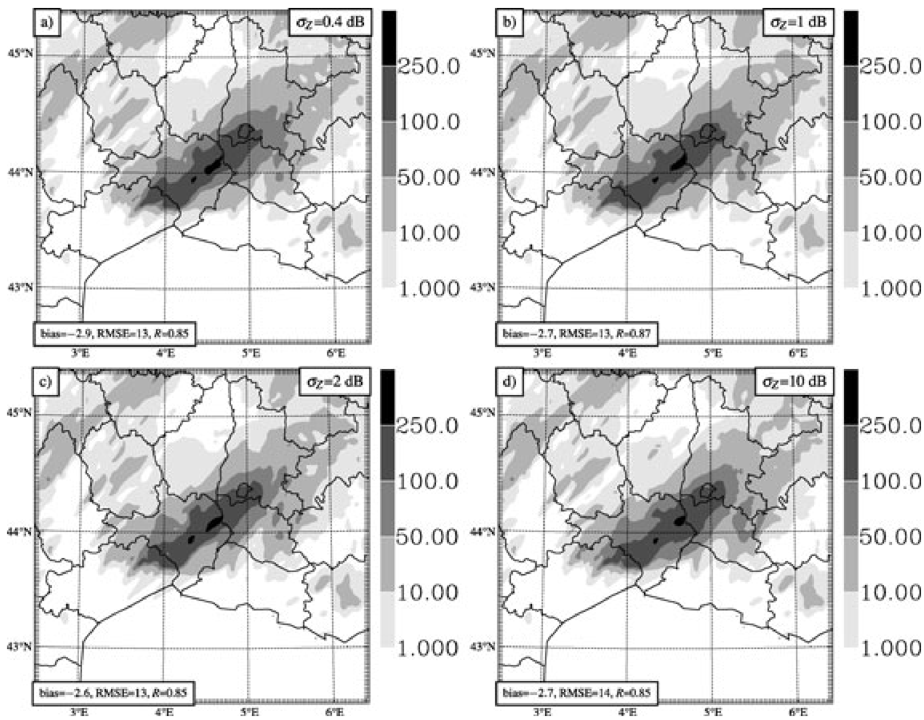

Fig. 13. Six-hour accumulated rainfall (mm) between 1500 UTC and 2100 UTC on 8 September 2002 from RAD15 with σ_Z varying from .4 to 10 dB. See text for the names of the simulations and parameters.

and that has been shown to be essential to obtain proper forecasts. The question addressed here is to know whether a cold pool can be generated during the forecast when the 1D+3DVar assimilation of reflectivity data is applied alone, that is, without assimilation of surface data. Two new experiments have been designed exactly the same as REF12 and RAD12, respectively, except that no surface data are assimilated at 1200 UTC. They are hereafter referred to as REFWS12 and RADWS12 (for REFerence or RADar Without Surface) (see Fig. 5).

In REF12, the description of the cold pool under the storm in the initial state is close to the observations, because of the assimilation of surface data (Figs. 14a and b). In contrast, when no observations directly related to the cold pool are assimilated, no intense cold pool is represented (Figs. 14c and d). This holds true for both experiments REFWS12 and RADWS12. The simulation starting from the REFWS12 analysis is not able to create a cold pool that matches the observations (compare Figs. 9a and 14e, at 1900 UTC). The updrafts therefore occur close to the Cévennes mountain foothills. The simulation starting from the RADWS12 analysis is able to create a cold pool, in spite of an initial state very close to that of REFWS12 in the low levels of the atmosphere (Fig. 14f). Even though of smaller extension than in RAD12, this cold pool forces updrafts to occur a bit upstream of the Cévennes foothills.

As a result, accumulated precipitation is better predicted by RADWS12 than by REFWS12: in RADWS12, maximum precipitation is located between that in REFWS12 and in RAD12 (Fig. 15, to compare with 6a). In particular, the

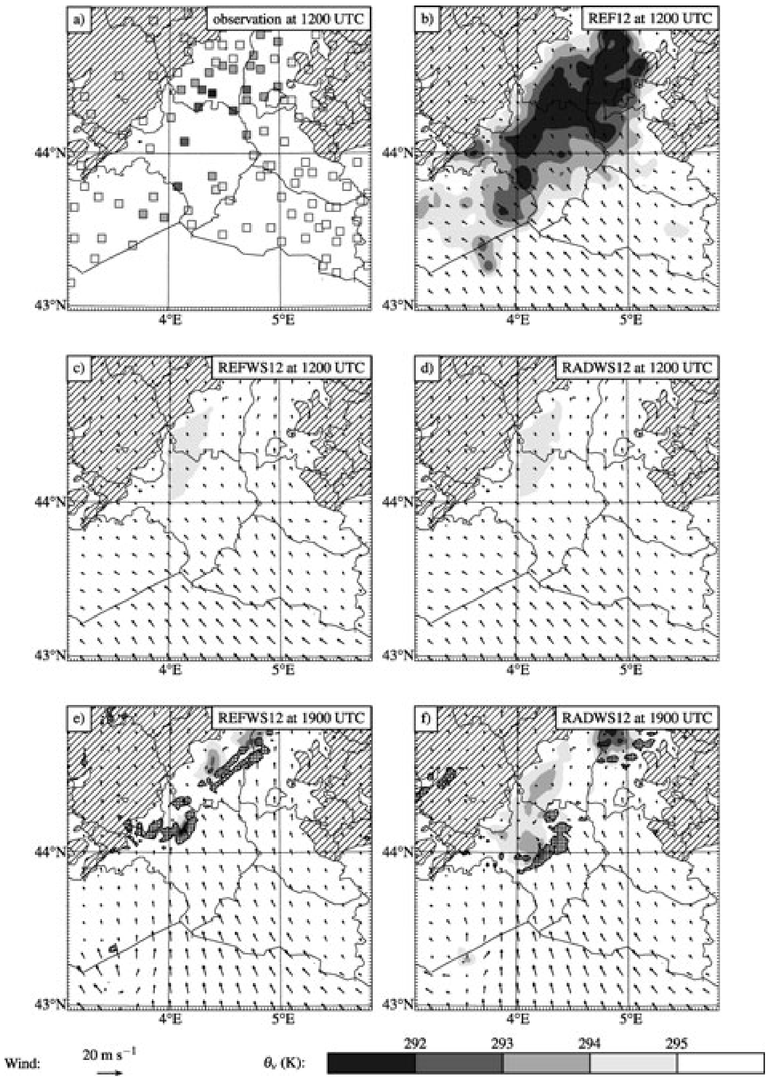

Fig. 14. (a) Virtual potential temperature (θ_v, in K) at 2 m AGL observed by the mesonet network at 1200 UTC. Simulated virtual potential temperature (θ_v, in K) at 2 m AGL, vertical velocity greater than 1 m s^{-1} at 2 km MSL (square hatch), and 10-m wind on 8 September 2002: (b–d) at 1200 UTC (analyses); (e–f) at 1900 UTC. Diagonal hatch: same as in Fig. 9.

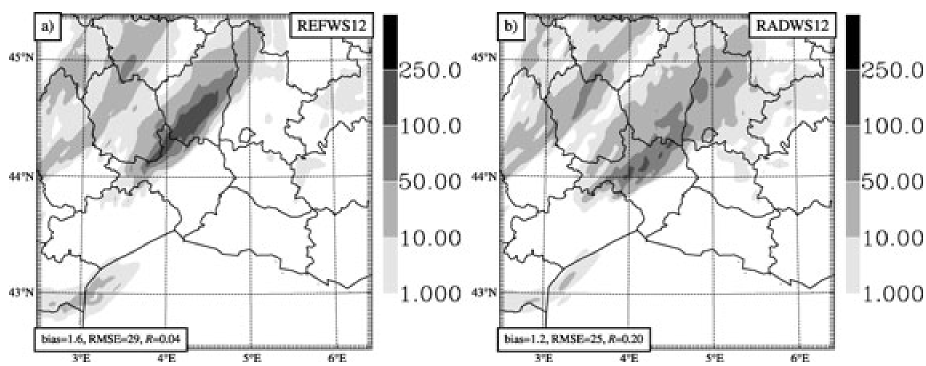

Fig. 15. Same as Fig. 6, but for (a) REFWS12 and (b) RADWS12.

correlation coefficient is highly improved, which reflects a better location of the precipitation pattern, and both ETS and FBIAS are better for all thresholds (Fig. 16). It shows that the assimilation of radar reflectivity data alone also leads to the physical process chain described in Section 4.2 (moistening of middle troposphere → intensification of precipitation → evaporation in subsaturated low layers → formation or sustainment of a cold pool) even when no cold pool is present in the initial state.

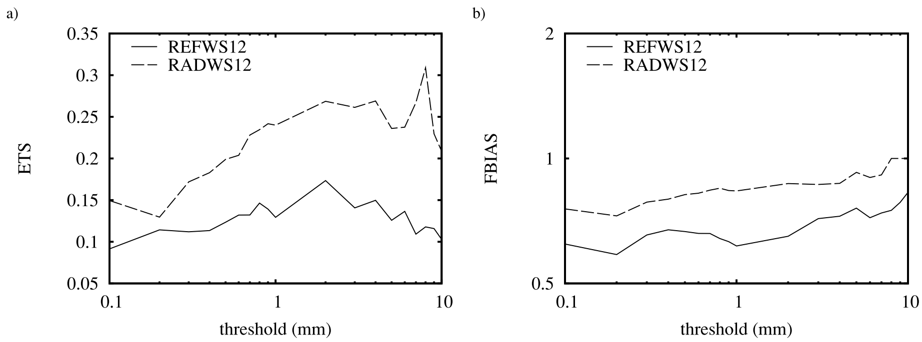

Fig. 16. Same as Fig. 7, but for REFWS12 and RADWS12.

6. Results from pre-operational runs

The 1D+3DVar method has been implemented and adapted in the Arome system, whose configuration is a 3-h Rapid Update Cycle (RUC) with eight daily updates (a 3-h forecast is used as background state for the next assimilation step). The Arome model was declared fit for operational use at Météo-France on 18 December 2008 and the assimilation of reflectivity data has since then been tested in a pre-operational configuration over assimilation periods of several days. Some results from such an experiment, which has been running from 15 April 0000 UTC to 23 April 2009 0000 UTC, are shown hereafter. For a comparison, two experiments have been run. In the first experiment, hereafter referred to as CTRL, conventional data such as radiosoundings, radiances (ATOVS, SEVIRI, SSM/I, etc.), temperature and humidity at 2 m, wind at 10 m, Doppler velocity from 16 radars of the French operational radar network, and GPS zenith total delay are assimilated (Yan et al., 2009). The second experiment referred as REFL, includes additional reflectivity data, which are assimilated through the 1D+3DVar method described above.

During this period, important precipitation associated with a surface cold front has crossed France eastwards on 16 April. Associated with a large low on the Near Atlantic, which was getting close to France during this time, the air mass was unstable over France. Associated with the cold upper-air low and front over France, embedded and post-frontal convective precipitation occurred during several days. A positive impact of the assimilation of reflectivity data is found in very short-range precipitation forecast scores. Here are shown results for 6-h accumulated precipitation forecasts against rain gauges, between 3- and 9-h forecasts, for daily runs starting at 0000 UTC and 1200 UTC. Different scores of model precipitation against rain gauges for different thresholds have been computed for these two experiments CTRL and REFL (Fig. 17). These short-term forecasts show improvement through the ETS, which increases in the REFL experiment. Also, the probability of detection (POD) is slightly improved for all thresholds, while the false alarm ratio (FAR) is also reduced for heavy and weak precipitation.

7. Summary and discussion

An original two-step method has been developed to assimilate reflectivity data into a cloud-resolving atmospheric model. This method, called 1D+3DVar, first converts reflectivity into humidity through a 1-D vertical retrieval method based on the physical consideration that modifying moisture is more important than modifying hydrometeor contents. Then, the obtained vertical profiles of relative humidity are assimilated with a conventional 3DVar assimilation system.

It has been shown through an OSSE that the 1-D retrieval method is able to produce humidity vertical profiles, which are consistent with observations. In particular, the method proved to be able to add, remove and displace signatures in humidity of convective cells according to the 'true' state of the atmosphere, which is perfectly known in such idealized experiments.

With real reflectivity observations, and for a particularly complex case study, the whole 1D+3DVar assimilation method has shown to be able to improve the dynamics of the convective system and the QPF. The assimilation of reflectivity data has moistened the middle troposphere, which has caused the formation of more precipitation. A part of this precipitation has evaporated near the ground, which has contributed to sustain and enhance the cold pool under the storm that forces upward lifting. Another part of this precipitation has reached the ground, which has contributed to improve the forecasted rainfall totals. Performing a 3-h assimilation cycle at the 1-h frequency has helped improve further QPF.

The sensitivity of this assimilation method to different configurations has also been investigated for this complex case. It has been shown that changes in the value of the standard deviation of observation and observation operator errors (σ_Z) had a very small impact on QPF. It has also been found that assimilating reflectivity data alone without assimilation of surface data allowed the numerical model to create a cold pool after a few hours, whereas no cold pool is present in the initial state. In contrast, the reference experiment, without assimilation of reflectivity nor surface data, is not able to create such a cold pool. This cold pool has an important, positive impact on the QPF in that it shifts the precipitation pattern

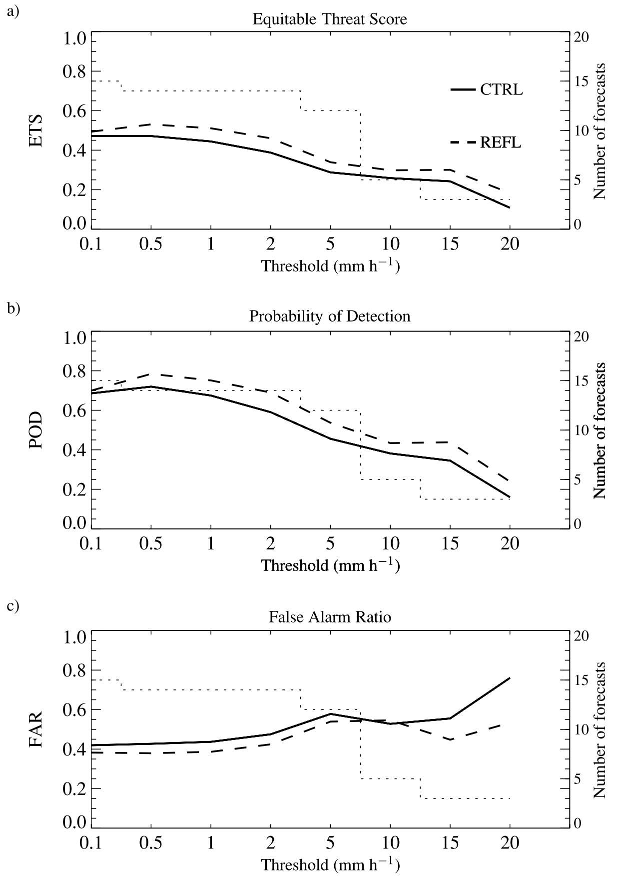

Fig. 17. (a) ETS, (b) POD and (c) FAR for 6-h accumulated precipitation forecasts against rain gauges, between 3- and 9-h forecasts (starting each day at 0000 UTC and 1200 UTC, from 0000 UTC, 15 April to 0000 UTC, 23 April 2009), as a function of threshold (mm h^{-1}), for CTRL (thick solid line) and REFL (thick dashed line). The thin dashed line represents the number of forecasts taken into account in calculations, that is, for which the number of observations above threshold exceeds 30.

towards its actual location, in comparison with the reference experiment.

This method has been adapted to the Arome assimilation system and it has been shown for an 8-d-long assimilation period with 3-h update cycles that it yielded positive results on short-term QPF. It is currently on its way of being included in the next Arome operational release.

8. Acknowledgments

The authors wish to thank Laurent Labatut for his assistance in this study. Thanks also go to François Bouttier for useful discussions in the early stages of this work. The authors are grateful to the anonymous reviewers who gave valuable suggestions.

References

Arnold, C. P. Jr., and Dey, C. H. 1986. Observing-systems simulation experiments: past, present, and future. *Bull. Am. Meteor. Soc.* **67**(6), 687–695. doi:10.1175/1520-0477(1986)067<0687:OSSEPP>2.0.CO;2.

Berre, L. 2000. Estimation of synoptic and mesoscale forecast error covariances in a limited-area model. *Mon. Wea. Rev.* **128**(3), 644–667. doi:10.1175/1520-0493(2000)128<0644:EOSAMF>2.0.CO;2.

Bielli, S. and Roux, F. 1999. Initialization of a cloud-resolving model with airborne Doppler radar observations of an oceanic tropical convective system. *Mon. Wea. Rev.* **127**(6), 1038–1055. doi:10.1175/1520-0493(1999)127<1038:IOACRM>2.0.CO;2.

Bouttier, F. 2003. The AROME mesoscale project, *Proceedings of the 2003 ECMWF Seminar on Recent Developments in Data Assimilation for Atmosphere and Ocean*, Reading, United Kingdom. http://www.ecmwf.int/publications/library/do/references/show?id=86068.

Bouttier, F. 2007. Arome, avenir de la prévision régionale (Arome, a next fine-scale numerical weather prediction model). *La Météorologie* **58**, 12–20 (in French).

Caumont, O., Ducrocq, V., Delrieu, G., Gosset, M., Parent du Châtelet, J. and co-authors. 2006. A radar simulator for high-resolution non-hydrostatic models. *J. Atmos. Oceanic Technol.* **23**(8), 1049–1067. doi:10.1175/JTECH1905.1.

Chancibault, K., Anquetin, S., Ducrocq, V. and Saulnier, G.-M. 2006. Hydrological evaluation of high-resolution precipitation forecast of the Gard flash-flood event (8–9 September 2002). *Quart. J. Roy. Meteor. Soc.* **132**, 1091–1117. doi:10.1256/qj.04.164.

Delrieu, G., Creutin, J.-D. and Andrieu, H. 1995. Simulation of radar mountain returns using a digitized terrain model. *J. Atmos. Oceanic Technol.* **12**(5), 1038–1049. doi:10.1175/1520-0426(1995)012<1038:SORMRU>2.0.CO;2.

Delrieu, G., Ducrocq, V., Gaume, É., Nicol, J., Payrastre, O. and co-authors. 2005. The catastrophic flash-flood event of 8–9 September 2002 in the Gard region, France: a first case study for the Cévennes-Vivarais Mediterranean Hydrometeorological Observatory. *J. Hydrometeor.* **6**(1), 34–52. doi:10.1175/JHM-400.1.

Ducrocq, V., Lafore, J.-P., Redelsperger, J.-L. and Orain, F. 2000. Initialization of a fine-scale model for convective-system prediction: a case study. *Quart. J. Roy. Meteor. Soc.* **126**(570), 3041–3065. doi:10.1002/qj.49712657004.

Ducrocq, V., Ricard, D., Lafore, J.-P. and Orain, F. 2002. Storm-scale numerical rainfall prediction for five precipitating events over France: on the importance of the initial humidity field. *Wea. Forecast.* **17**(6), 1236–1256. doi:10.1175/1520-0434(2002)017<1236:SSNRPF>2.0.CO;2.

Ducrocq, V., Nuissier, O., Ricard, D., Lebeaupin, C. and Thouvenin, T. 2008. A numerical study of three catastrophic precipitating events over southern France. II: mesoscale triggering and stationarity factors. *Quart. J. Roy. Meteor. Soc.* **134**(630), 131–145. doi:10.1002/qj.199.

Fischer, C., Montmerle, T., Berre, L., Auger, L. and Ştefănescu, S. E. 2005. An overview of the variational assimilation in the ALADIN/France numerical weather-prediction system. *Quart. J. Roy. Meteor. Soc.* **131**(613), 3477–3492. doi:10.1256/qj.05.115.

Hu, M., Weygandt, S. S., Xue, M. and Benjamin, S. G. 2007. Development and testing of a new cloud analysis package using radar, satellite, and surface cloud observations within GSI for initializing

Rapid Refresh, In: *Proceedings of the 22nd Conf. on Weather Analysis and Forecasting/18th Conf. on Numerical Weather Prediction*, Amer. Meteor. Soc., Park City, UT. Abstract no. P2.5.

Jaubert, G., Auger, L., Colombon, N., Ducrocq, V. and Bouttier, F. 2005. Meso-gamma 3D-Var assimilation of surface measurements on heavy rain events: impact on short range high resolution simulations, *World Weather Research Programme Symposium on Nowcasting and Very Short Range Forecasting (WSN05)*, Toulouse, France. Abstract no. 3.15.

Jones, C. D. and Macpherson, B. 1997. A latent heat nudging scheme for the assimilation of precipitation data into an operational mesoscale model. *Meteorol. Appl.* **4**, 269–277.

Kim, M.-J., Weinman, J. A., Olson, W. S., Chang, D.-E., Skofronick-Jackson, G. and co-authors. 2008. A physical model to estimate snowfall over land using AMSU-B observations. *J. Geophys. Res.* **113**(D09201). doi:10.1029/2007JD008589.

Kummerow, C., Olson, W. S. and Giglio, L. 1996. A simplified scheme for obtaining precipitation and vertical hydrometeor profiles from passive microwave sensors. *IEEE Trans. Geosci. Remote Sens.* **34**(5), 1213–1232. doi:10.1109/36.536538.

Kummerow, C., Hong, Y., Olson, W. S., Yang, S., Adler, R. F. and co-authors. 2001. The evolution of the Goddard profiling algorithm (GPROF) for rainfall estimation from passive microwave sensors. *J. Appl. Meteor.* **40**(11), 1801–1820. doi:10.1175/1520-0450(2001)040<1801:TEOTGP>2.0.CO;2.

Lafore, J.-P., Stein, J., Asencio, N., Bougeault, P., Ducrocq, V. and co-authors. 1998. The meso-NH atmospheric simulation system. Part I: adiabatic formulation and control simulations. Scientific objectives and experimental design. *Ann. Geophys.* **16**(1), 90–109.

Lin, Y., Ray, P. S. and Johnson, K. W. 1993. Initialization of a modeled convective storm using Doppler radar-derived fields. *Mon. Wea. Rev.* **121**(10), 2757–2775. doi:10.1175/1520-0493(1993)121<2757:IOAMCS>2.0.CO;2.

Lindskog, M., Salonen, K., Järvinen, H. and Michelson, D. B. 2004. Doppler radar wind data assimilation with HIRLAM 3DVAR. *Mon. Wea. Rev.* **132**(5), 1081–1092. doi:10.1175/1520-0493(2004)132<1081:DRWDAW>2.0.CO;2.

Lopez, P. and Bauer, P. 2007. "1D+4DVAR" assimilation of NCEP Stage-IV radar and gauge hourly precipitation data at ECMWF. *Mon. Wea. Rev.* **135**(7), 2506–2524. doi:10.1175/MWR3409.1.

Lorenc, A. C. 1986. Analysis methods for numerical weather prediction. *Quart. J. Roy. Meteor. Soc.* **112**, 1177–1194.

Marécal, V. and Mahfouf, J.-F. 2002. Four-dimensional variational assimilation of total column water vapour in rainy areas. *Mon. Wea. Rev.* **130**(1), 43–58. doi:10.1175/1520-0493(2002)130<0043:FDVAOT>2.0.CO;2.

Marécal, V. and Mahfouf, J.-F. 2003. Experiments on 4D-Var assimilation of rainfall data using an incremental formulation. *Quart. J. Roy. Meteor. Soc.* **129**(594), 3137–3160. doi:10.1256/003590003769682219.

Montmerle, T. and Faccani, C. 2009. Mesoscale assimilation of radial velocities from Doppler radar in a pre-operational framework. *Mon. Wea. Rev.* **137**(6), 1939–1953. doi:10.1175/2008MWR2725.1.

Nagarajan, B., Yau, M. K. and Fillion, L. 2006. A numerical study of the 1996 Saguenay flood cyclone: Effect of assimilation of precipitation data on quantitative precipitation forecasts. *Mon. Wea. Rev.* **134**(5), 1371–1388. doi:10.1175/MWR3128.1.

Nuissier, O., Ducrocq, V., Ricard, D., Lebeaupin, C. and Anquetin, S. 2008. A numerical study of three catastrophic precipitating events over southern France. I: numerical framework and synoptic ingredients. *Quart. J. Roy. Meteor. Soc.* **134**(630), 111–130. doi:10.1002/qj.200.

Olson, W. S., Kummerow, C. D., Heymsfield, G. M. and Giglio, L. 1996. A method for combined passive-active microwave retrievals of cloud and precipitation profiles. *J. Appl. Meteor.* **35**(10), 1763–1789. doi:10.1175/1520-0450(1996)035<1763:AMFCPM>2.0.CO;2.

Olson, W. S., Kummerow, C. D., Hong, Y. and Tao, W.-K. 1999. Atmospheric latent heating distributions in the tropics derived from satellite passive microwave radiometer measurements. *J. Appl. Meteor.* **38**(6), 633–664. doi:10.1175/1520-0450(1999)038<0633:ALHDIT>2.0.CO;2.

Parent du Châtelet, J., Perier, L., Do Khac, K. and Roquain, P. 2001. Castor2: a new computer for the French radar network, *Proc. 30th Int Conf. on Radar Meteorology*, Amer. Meteor. Soc., Munich, Germany, 82–83.

Schelleng, J. C., Burrows, C. R. and Ferrell, E. B. 1933. Ultra-short-wave propagation. *Proc. IRE* **21**(3), 427–463.

Stephan, K., Klink, S. and Schraff, C. 2008. Assimilation of radar-derived rain rates into the convective-scale model COSMO-DE at DWD. *Quart. J. Roy. Meteor. Soc.* **134**(634), 1315–1326. doi:10.1002/qj.269.

Sun, J. and Crook, N. A. 1997. Dynamical and microphysical retrieval from Doppler radar observations using a cloud model and its adjoint. Part I: model development and simulated data experiments. *J. Atmos. Sci.* **54**(12), 1642–1661. doi:10.1175/1520-0469(1997)054<1642:DAMRFD>2.0.CO;2.

Tong, M. and Xue, M. 2005. Ensemble Kalman Filter assimilation of Doppler radar data with a compressible nonhydrostatic model: OSS experiments. *Mon. Wea. Rev.* **133**(7), 1789–1807. doi:10.1175/MWR2898.1.

Xiao, Q., Kuo, Y.-H., Sun, J., Lee, W.-C., Lim, E. and co-authors. 2005. Assimilation of Doppler radar observations with a regional 3DVAR system: impact of Doppler velocities on forecasts of a heavy rainfall case. *J. Appl. Meteor.* **44**, 768–788. doi:10.1175/JAM2248.1.

Xiao, Q., Kuo, Y.-H., Sun, J., Lee, W.-C., Barker, D. M. and co-authors. 2007. An approach of radar reflectivity data assimilation and its assessment with the inland QPF of typhoon Rusa (2002) at landfall. *J. Appl. Meteor. Climatol.* **46**(1), 14–22. doi:10.1175/JAM2439.1.

Xue, M., Tong, M. and Droegemeier, K. K. 2006. An OSSE framework based on the ensemble square root Kalman filter for evaluating the impact of data from radar networks on thunderstorm analysis and forecasting. *J. Atmos. Oceanic Technol.* **23**(1), 46–66. doi:10.1175/JTECH1835.1.

Yan, X., Ducrocq, V., Jaubert, G., Brousseau, P., Poli, P. and co-authors. 2009. The benefit of GPS zenith delay assimilation to high-resolution quantitative precipitation forecasts: a case-study from COPS IOP 9. *Quart. J. Roy. Meteor. Soc.* doi:10.1002/qj.508.

Zhao, Q. and Jin, Y. 2008. High-resolution radar data assimilation for hurricane Isabel (2003) at landfall. *Bull. Am. Meteor. Soc.* **89**(9), 1355–1372. doi:10.1175/2008BAMS2562.1.